OBSERVATION and SIMULATIONS of WATER VAPOR TURBULENCE PROFILES in CONVECTIVE BOUNDARY LAYERS OVER the ARM SOUTHERN GREAT PLAINS and TROPICAL WESTERN PACIFIC SITES

ARM ASR PI Meeting, 13-16 Mar 2017, Vienna, VA

[1]M. K. Osman, [2]T. Heus, [3]D. D. Turner, [4]R. Newsom, [2]R. White

[1]CIMSS University of Oklahoma, Norman, OK; [2]Department of Physics, Cleveland State University, Cleveland, OH;

[3]NOAA Earth System Research Laboratory Global Systems Division, Boulder, CO; [4]Pacific Northwest National Laboratory, Richland, WA

- ❖ Water vapor turbulence is derived from observations and LES modeling
- ❖ Turbulent profiles were computed from the TWP Raman lidar located at Darwin, Australia from 62 cases, comprising of 13 monsoon and 49 non-monsoon events
- ❖ Median of the water vapor variance profile is larger in the monsoon events than in the non-monsoon, and neither agrees well with median variance profile from the SGP.
- ❖ The coefficient of the structure function profiles, which is related to molecular dissipation rate, in monsoon events is also found to be larger than during the non-monsoon.
- ❖ LES simulations show a discrepancy between the humidity distributions based on spatial versus temporal statistics, especially in the higher order statistics.
- ❖ The sub-gaussian kurtosis at the top of the CBL that was reported from observations (McNicholas and Turner 2014) can be reproduced in the temporal LES statistics, but not in the spatial statistics.
- ❖ The difference between spatial and temporal statistics can be fully explained by high kurtosis values (>~5) in the spatial distribution of the top-down scalar
- ❖ This is attributed to relatively rare but long lasting entrainment events (dry tongues, Couvreux et al 2007), which cause a bias in the temporal statistics.

TWP Raman Lidar Observations

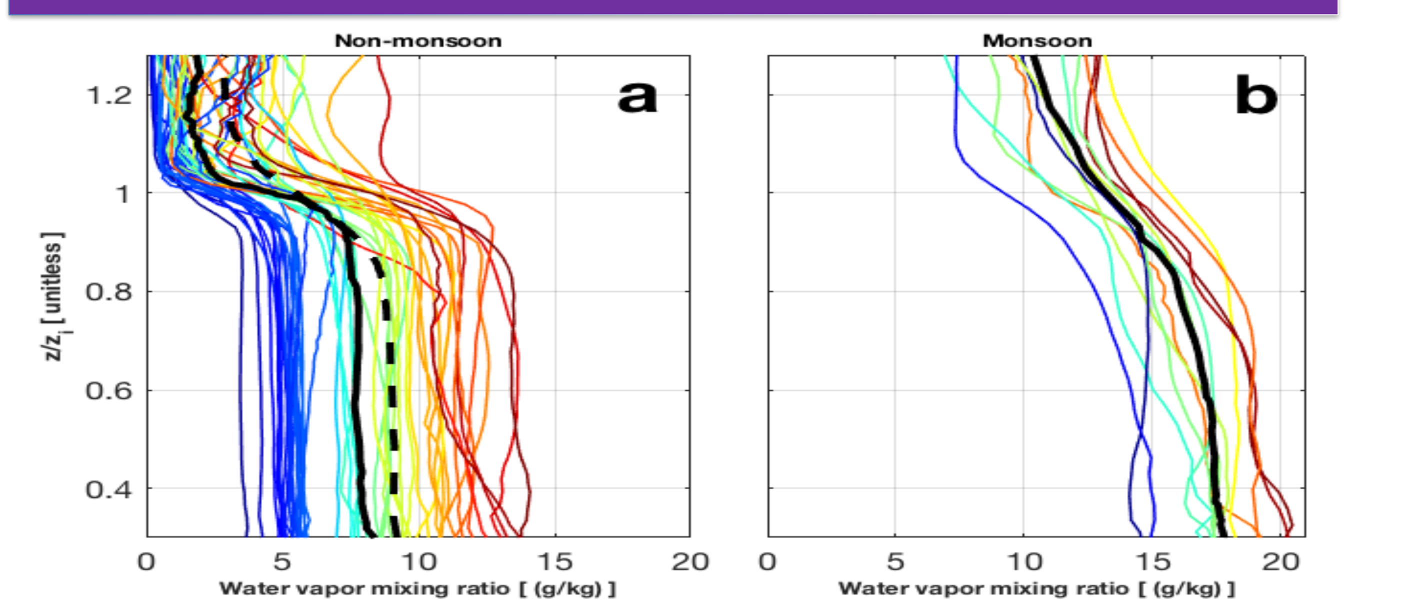

Mean water vapor mixing ratio profiles for each 2 h period for (a) non-monsoon and (b) monsoon. The dark dashed line in Fig 1a is the median of water vapor profile at the SGP taken from Turner et al. [2014] and the solid dark lines are the median profiles in monsoon and non-monsoon.

- ❖ Profiles are nearly constant from 0.3-0.8 z_i & decreases above 0.8 z_i due to mixing
- ❖ Profiles in the non-monsoon cases decrease fast above z_i unlike in monsoon cases
- ❖ Median of water vapor from the non-monsoon cases is more similar to the SGP

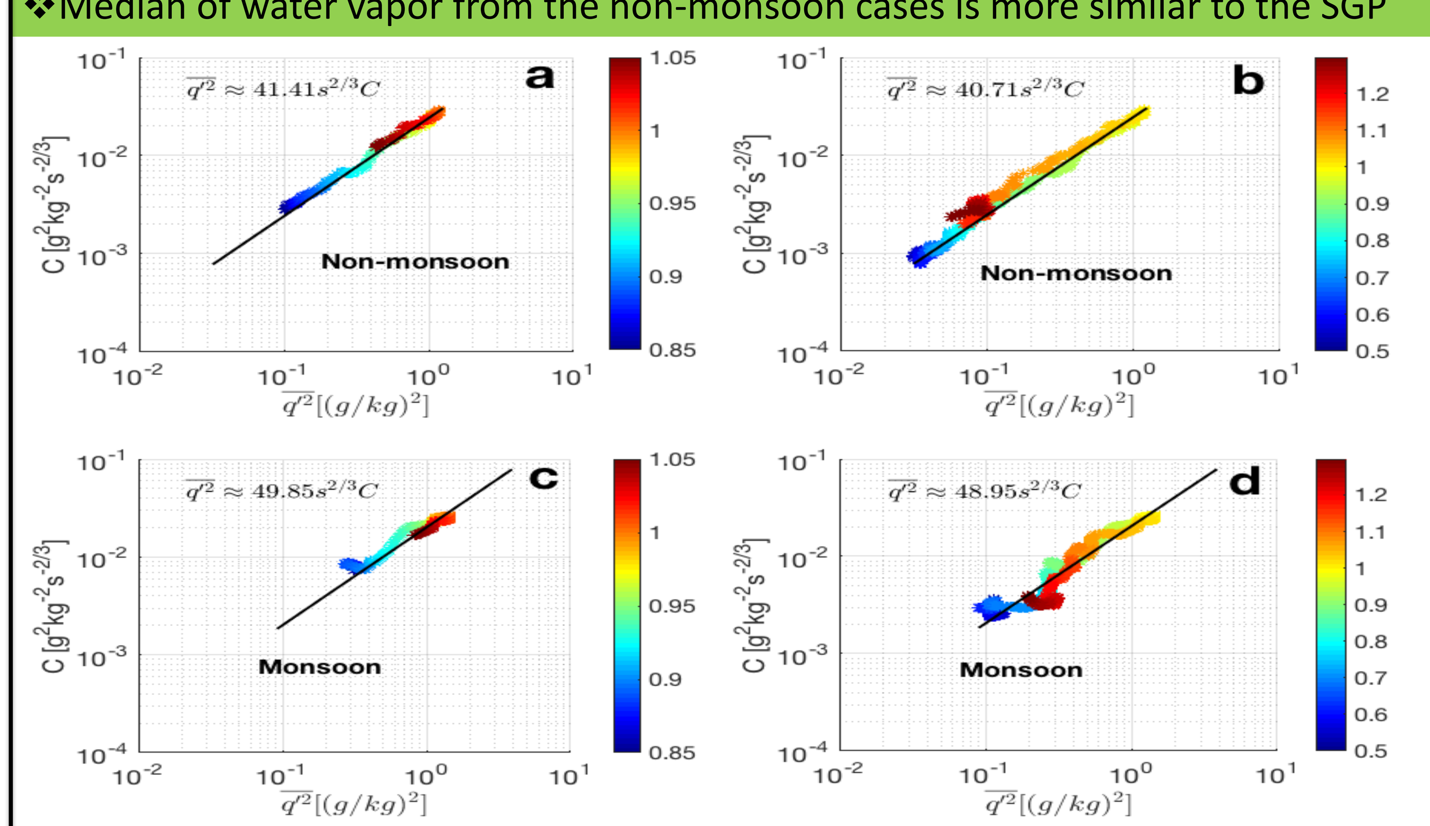

Relationship between the atmospheric variance and the coefficient of the structure function for the median profiles shown above for non-monsoon (a, b) and monsoon (c, d) events. The linear fits were performed over the altitude ranges 0.85-1.05 z_i and 0.5-1.03 z_i in the left (a, c) and right panels (b, d), respectively.

- ❖ The slope in the monsoon is larger than the slope during the non-monsoon
- ❖ Larger variance leads to larger destruction rate of variance [Wulfmeyer et al. 2016]

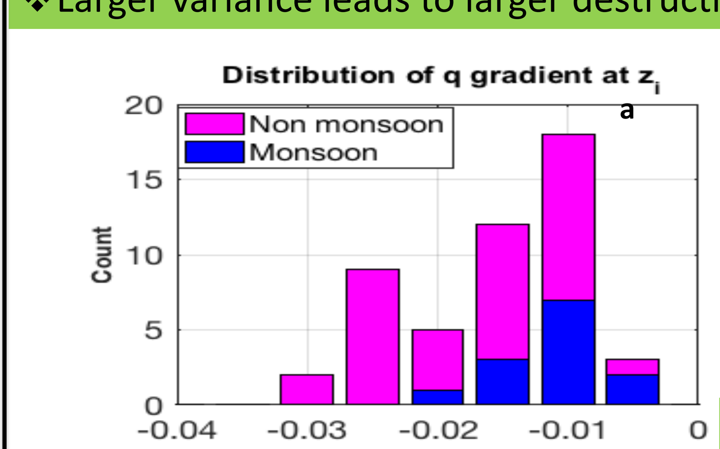

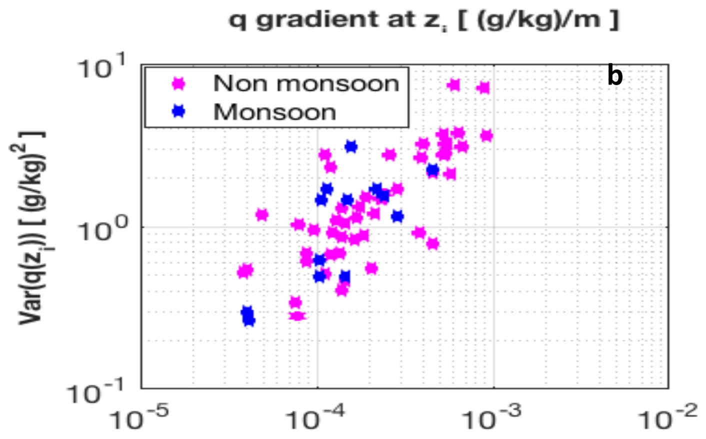

- ❖ The relationship between water vapor variance at z_i and the square of the gradient of water vapor mixing ratio at z_i [Sorbjan 2005]

$$\overline{q'^2}(z_i) = c_q w_* g_i^2 / N_i^2 \qquad g_i = \left.\frac{d\overline{q}}{dz}\right|_{z_i}$$

- ❖ N_i is the Brunt-Vaisala frequency in the interfacial layer, w_* is the convective velocity scale and c_q is a constant
- ❖ Correlation coefficients were found to be 0.73 and 0.80 for monsoon and non-monsoon seasons, respectively
- ❖ After removing a single case in the monsoon events that is more than two standard deviations from the mean.

The distribution of the vertical gradient in water vapor mixing ratio at z_i (a) and the atmospheric variance at z_i as a function of the square of the gradient of water vapor mixing ratio at z_i (b).

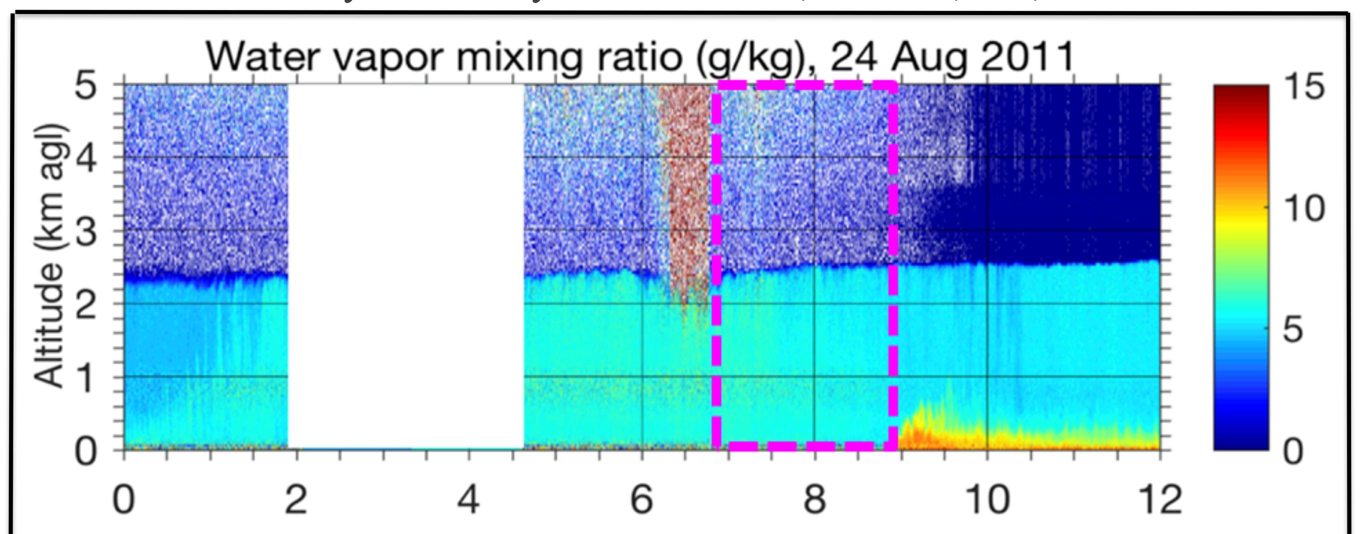

Time-height cross-section of water vapor mixing (g kg^{-1}) from Raman lidar at Darwin, Australia. The data have 10-s and 37.5 m resolutions

- ❖ Well mixed and quasi-stationary CBL for 2 hours; 0650-0850 UTC
- ❖ LT=UTC+0930
- ❖ Sunset ~0930 UTC
- ❖ Solar noon ~0300 UTC

Assuming that the atmospheric variance, $\overline{q'^2}$, is mainly as a result of isotropic turbulence within inertial subrange (*Monin and Yaglom* 1979), the ACF at lag τ, $M_{11}(\tau)$, can be approximated as

$$M_{11}(\tau) = \overline{q'^2} - C\tau^{2/3}$$

where C is a parameter that contains both the eddy dissipation and the scalar variance dissipation

- ❖ Variance and the coefficient of the structure function profiles in the monsoon is larger
- ❖ Variance of the non-monsoon & the SGP are equal between 0.3-0.75 z_i
- ❖ Variance of the monsoon & the SGP are equal between 0.9-1.1 z_i
- ❖ Skewness profiles show a transition from negative to positive just below z_i

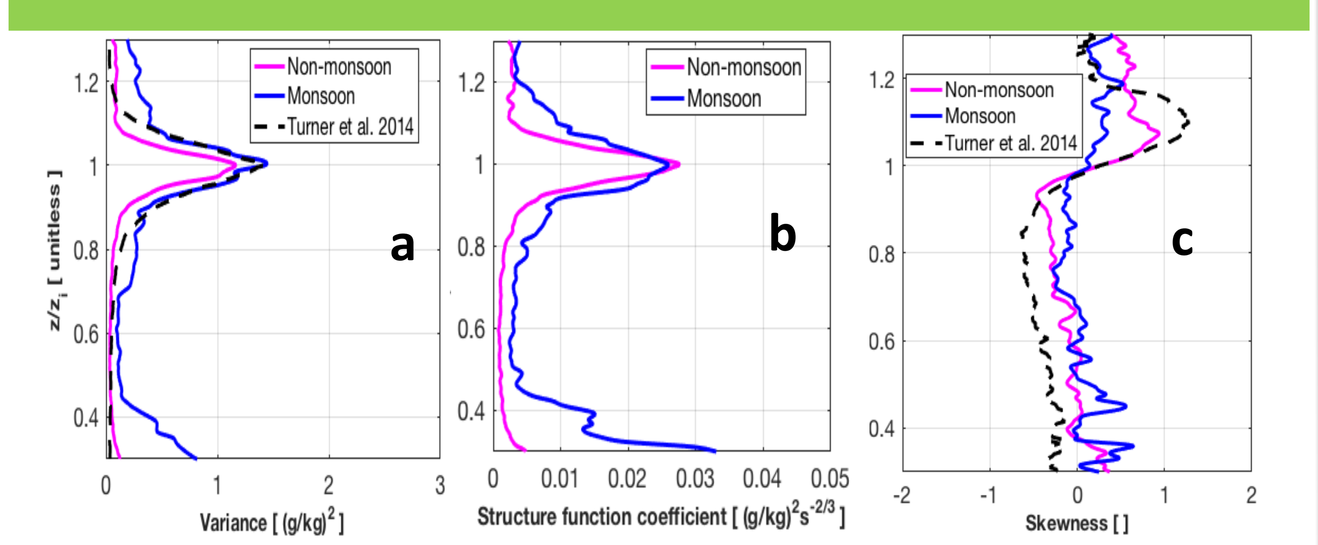

Median the profiles of atmospheric water vapor variance (a), coefficient of the structure function (b) and skewness (c) derived from monsoon and non-monsoon cases. The dashed dark line is the median variance profile at the SGP taken from Turner et al. [2014].

LES simulations: Spatial vs Temporal

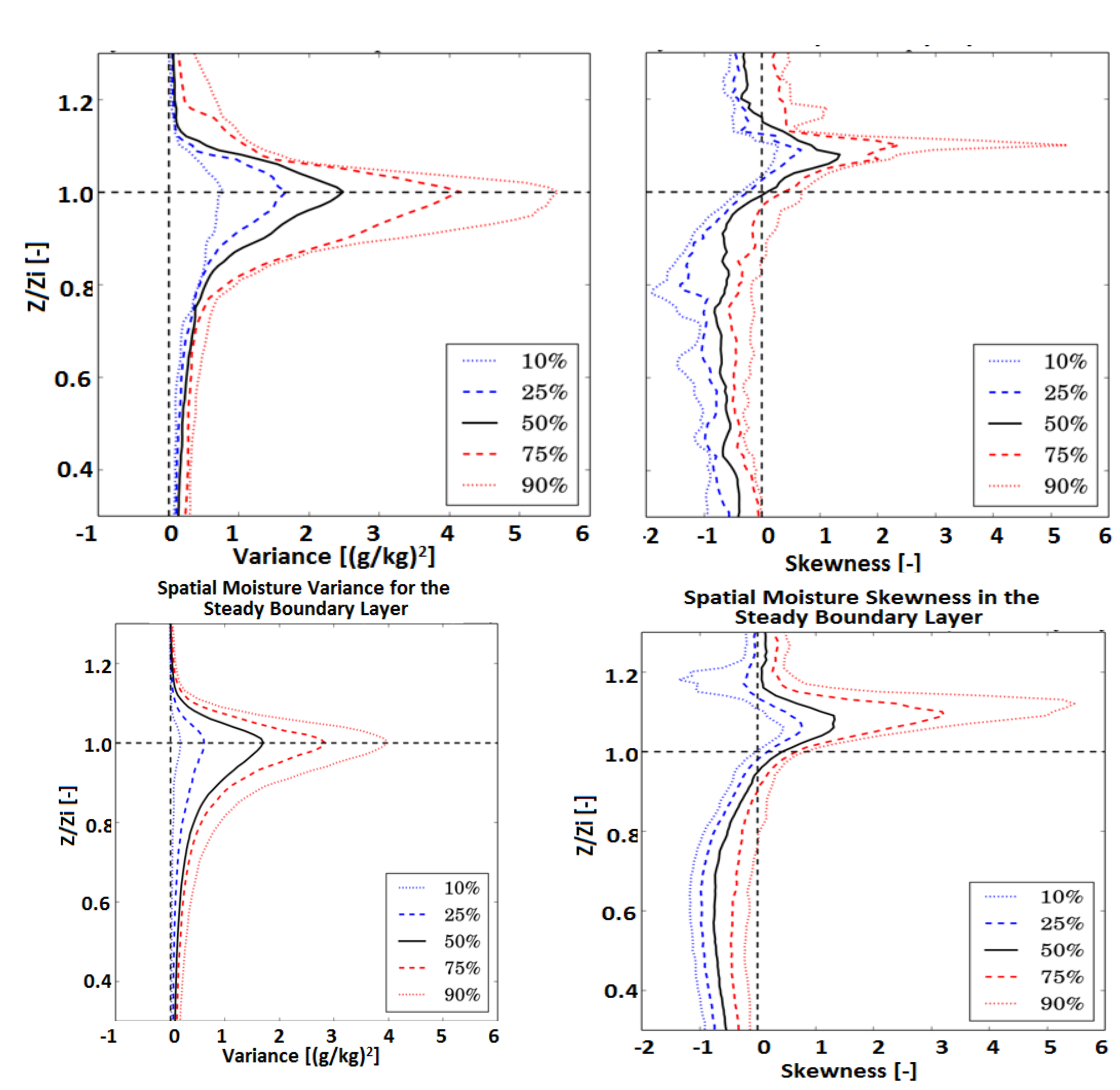

Top: Temporally averaged water vapor moments from LES
Bottom: Same, but spatially averaged

- ❖ LES simulations driven by ARM variational analysis (Xie et al, 2004) are well able to reproduce water vapor moments (Turner et al, 2014)
- ❖ However, moments are not the same between spatial and temporal averaging. How come?

LES cloud size distributions

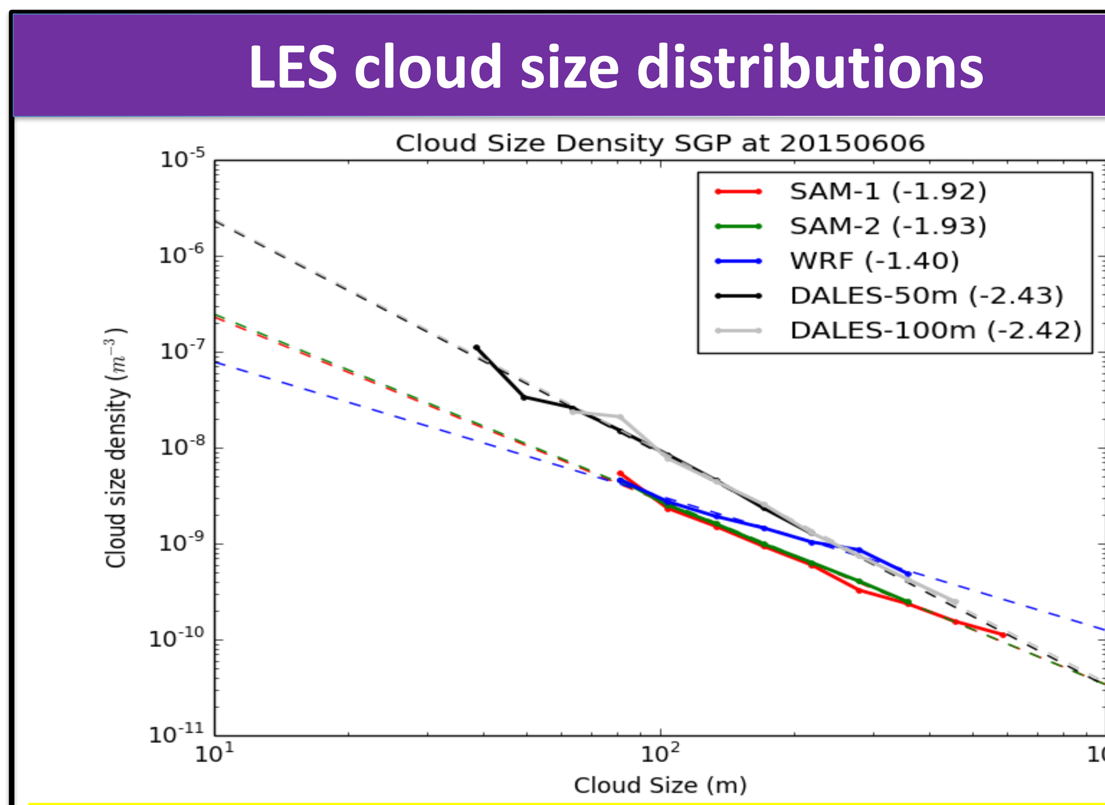

Cloud size distribution produced from different LES simulations

- ❖ LES cloud size distributions between different LASSO simulations and own DALES simulations with different setting and initial conditions
- ❖ All runs show a power law
- ❖ The slope of the power law is not universal, and seems model dependent
- ❖ Initial conditions and driver details are less of a source of uncertainty

Higher moments at the top of the CBL

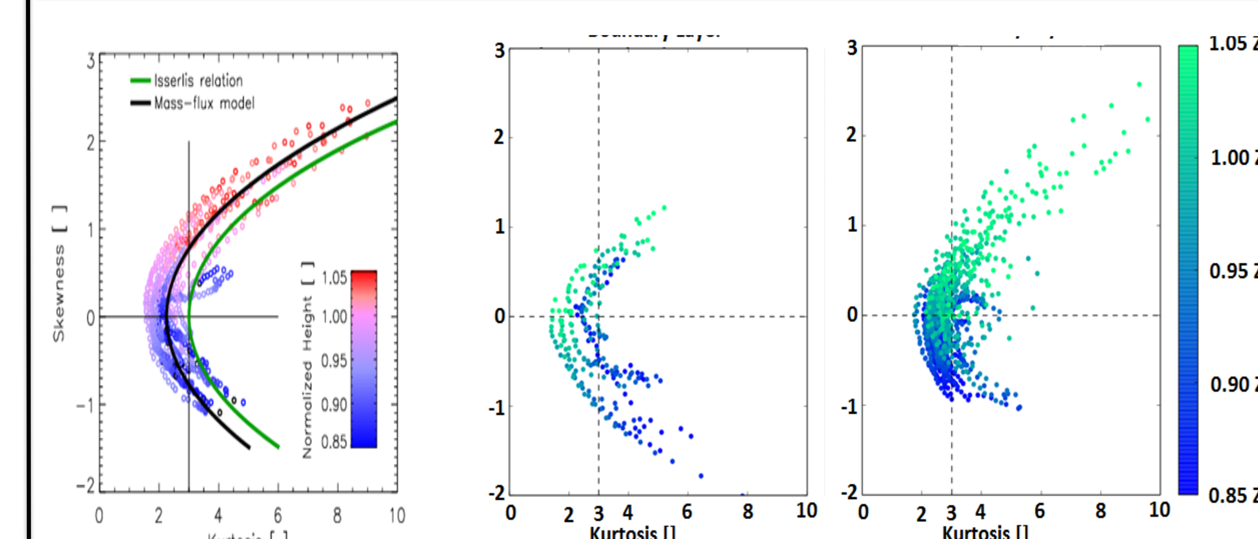

Kurtosis vs. Skewness: (Left) Observed; (Middle) Temporally based; (Right) Spatially based

- ❖ Just like with the variance, skewness and kurtosis of water vapor at BL top reproduces observations well
- ❖ The temporal statistics show kurtosis below 3 (Gaussian) at BL top
- ❖ Spatial statistics show kurtosis close to 3 at BL top.

- ❖ To understand the reason behind the discrepancy between temporal and spatial, we look at two artificial scalars:
  1) Bottom up: No initial value, just a surface flux; emphasizes thermal updrafts
  2) Top down: No surface flux, just an initial value above the BL; emphasizes entrainment events
- ❖ Any scalar (water vapor, temperature) behaves as a linear combination of these two scalars.

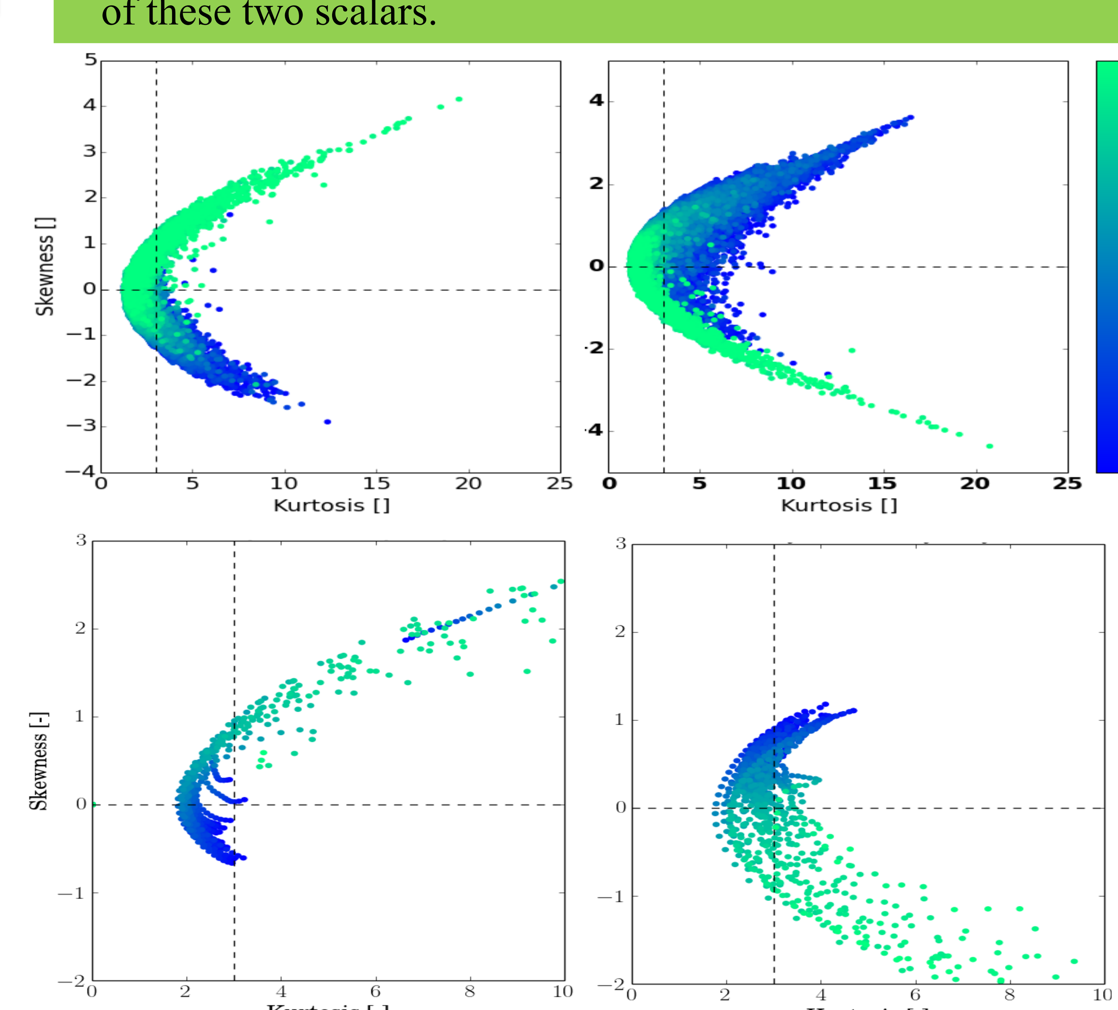

Kurtosis vs. Skewness: (top) Spatial averaging and (bottom) Temporal averaging using (left) the Bottom Up scalar, and (right) the Top Down scalar

- ❖ It is mostly the top down scalar (nr 2) that shows a strongly enhanced kurtosis in spatial statistics as compared with temporal
- ❖ We interpret that as persistent but local entrainment events, such as dry tongues (Couvreux et al 2007)
- ❖ Insufficient spatial sampling will likely miss those downdrafts, and alter higher order moments.

Acknowledgements

➢ This project is funded by award DE-SC0014375 of the Atmospheric System Research program of the Department of Energy
➢ We thank the Ohio Supercomputer Center for allocating the computational resources

Contacts: mohammed.osman@noaa.gov and t.heus@csuohio.edu